Arch. Metall. Mater. **65** (2020), 3, 1063-1067

DOI: 10.24425/amm.2020.133218

IL-KYU PARK[1], SANG-SEOK LEE[1], YONG KYOON MOK[2],
CHAN-WOO JEON[1], HYUN-GIL KIM[3*]

DYNAMIC CHARGE CARRIER TRANSPORT BEHAVIORS IN ZIRCONIUM OXIDE FOR NUCLEAR CLADDING MATERIALS

Dynamic charge carrier transport behavior in the zirconium (Zr) oxide was investigated based on the frequency-dependent capacitance-voltage (*C-V*) and temperature-dependent current-voltage (*I-V*) measurements. The Zr oxide was formed on the ZIRLO and newly developed zirconium-based alloy (NDZ) by corrosion in the PWR-simulated loop at 360°C. The corrosion test for 90 days showed that the NDZ exhibits better corrosion resistance than ZIRLO alloy. Based on the *C-V* measurement, dielectric constant values for the Zr oxide was estimated to be 11.28 and 11.52 for the ZIRLO and NDZ. The capacitance difference between low and high frequency was larger in the ZIRLO than in the NDZ, which was attributed to more mobile electrical charge carriers in the oxide layer on the ZIRLO alloy. The current through the oxide layers on the ZIRLO increased more drastically with increasing temperature than on the NDZ, which indicating that more charge trap sites exist in the ZIRLO than in NDZ. Based on the dynamic charge carrier transport behavior, it was concluded that the electrical charge carrier transport within the oxide layers was closely related with the corrosion behavior of the Zr alloys.

Keywords: Zirconium, Nuclear cladding, Zr oxide, Capacitance-voltage, Current-voltage

1. Introduction

For few decades, Zirconium (Zr)-based alloys have been achieved much attention for applications as a fuel cladding and other components of fuel assembly in nuclear reactors due to their excellent corrosion resistance, mechanical hardness, high melting temperature, and stability under the irradiation condition during nuclear reactor operation [1-5]. Especially, Zircaloy-4 (Zr-1.5Sn-0.2Fe0.1Cr in wt.%) is a Zr-based alloy containing a few percent of Sn, Fe, and Cr and has been developed for application in nuclear fuel cladding tubes [6]. Because of its high resistance to corrosion and stable under neutron irradiation, Zircaloy-4 has been used for a long time in commercial nuclear power plants. To further improve the performance of the Zr-based alloys, many parameters, such as safety, reliability, long-term stability, and economical operation have been considered. Recently, advanced Zr-based alloys containing high Nb content, such as ZIRLO (Zr-1Nb-1Sn-0.1Fe in wt.%), HANA-4 (Zr-1.5Nb-0.4Sn-0.2Fe-0.1Cr in wt.%) [8], and HANA-6 (Zr-1.1Nb-0.05Cu in wt.%) have been developed to meet the demands for increased fuel discharge burn-up and power level [7-8]. These excellent corrosion-resistance of the Zr-based alloys have been known to be attributed to the formation of stable Zr oxide on the surface [9,10]. The oxidation behavior of metal in aqueous ambient is dominated by the diffusion of oxidant species and electrical charge carrier [9-11]. To further investigate the oxidation behavior of the Zr-based alloys, the dynamic charge carrier transport behaviors through the Zr oxide should be fully understood. Therefore, in this study, we have investigated on the dynamic charge carrier transport behaviors in the Zr-based alloys based on the frequency-dependent capacitance-voltage and temperature-dependent current-voltage measurements. In addition, we have considered the relation between these dynamic charge carrier transport behaviors with the corrosion resistance.

2. Experimental

In this study, we compared the electrical properties of the Zr oxides for the conventional ZIRLO alloy and newly devel-

[1] SEOUL NATIONAL UNIVERSITY OF SCIENCE AND TECHNOLOGY, DEPARTMENT OF MATERIALS SCIENCE AND ENGINEERING, SEOUL, REPUBLIC OF KOREA
[2] KEPCO NUCLEAR FUEL, DAEJEON, REPUBLIC OF KOREA
[3] KOREA ATOMIC ENERGY RESEARCH INSTITUTE, NUCLEAR FUEL SAFETY RESEARCH DIVISION, 989-111 DAEDEOK-DAERO, YUSEONG-GU, DAEJEON 34057, REPUBLIC OF KOREA
* Corresponding author: hgkim@kaeri.re.kr

oped zirconium based alloy which containing over 95 wt% of Zr and additives. These samples will be noted as ZIRLO and NDZ in this manuscript. They were thermally annealed at 475°C to completely recrystallize the microstructures. To form the oxide layers on the Zr alloys, corrosion test was carried out based on the ASTM G2 procedure. The Zr alloy plates were cut into 20 mm × 25 mm × *t* mm size. And they were mechanically polished and cleaned by using acetone and ethanol in the ultrasonic bath for 10 min. The corrosion test was performed in the pressurized water reactor (PWR)-simulated loop at 360°C in 2.2 ppm Li solution. The corrosion tested samples were weighed periodically to check the weight gain. For the investigation of the electrical properties of the oxides before transition, the oxide used in this study was tested for 90 days.

To investigate the electrical properties of the oxides formed during the oxidation test, metal-insulator (oxide)-metal (MIM) capacitor structure was fabricated. As shown in Fig. 1(a), Zr alloys and aluminum metal were used for the bottom and top electrodes, respectively. The aluminum top electrode was deposited by using DC sputtering method through the circular shape of shadow mask. The diameter and thickness of the aluminum electrode were 0.5 mm and 200 nm, respectively.

To investigate the structural properties of the Zr oxide, X-ray diffraction (XRD, Rigaku D/Max-2500 diffractometer equipped with a Cu Ka source) was measured for the corrosion tested samples for 90 days. The electrical properties of the oxides were measured by using current-voltage (*I-V*) and capacitance-voltage (*C-V*) measurements. The *I-V* measurement were performed using a source meter (Keithley 2450) with variation of temperature by hot chuck from 20 to 100°C. The *C-V* measurement were performed using an impedance analyzer (Agilent 4292A) with voltage amplitude of –30 mV at the frequency of 10 kHz and 1 MHz.

3. Results and discussion

To investigate the electrical properties of the Zr oxide, corrosion test was performed for 90 days before starting transition. Figure 2(a) shows the corrosion test results for the ZIRLO and NDZ for 90 days. They showed similar and typical corrosion behavior of Zr alloys showing that the corrosion occurs drastically until 30 days and increase linearly by 90 days. Considering the weight gain, the oxide thickness for the ZIRLO and NDZ after 90 days assumed to be 2.12 and 2.06 μm, respectively. The corrosion test results imply that the NDZ exhibits better corrosion resistance. Figure 2(b) shows the XRD results for the samples after 90 days corrosion test. Two samples showed similar XRD features of the Zr oxide formed by corrosion. The XRD peaks are corresponding to the (111), (–111), (002), and (200) planes of the monoclinic phase of Zr oxide [12]. It should be noted that the tetragonal phase showed negligibly small peak even before the transition. The Zr oxides for both alloys were mainly consisted of monoclinic phase.

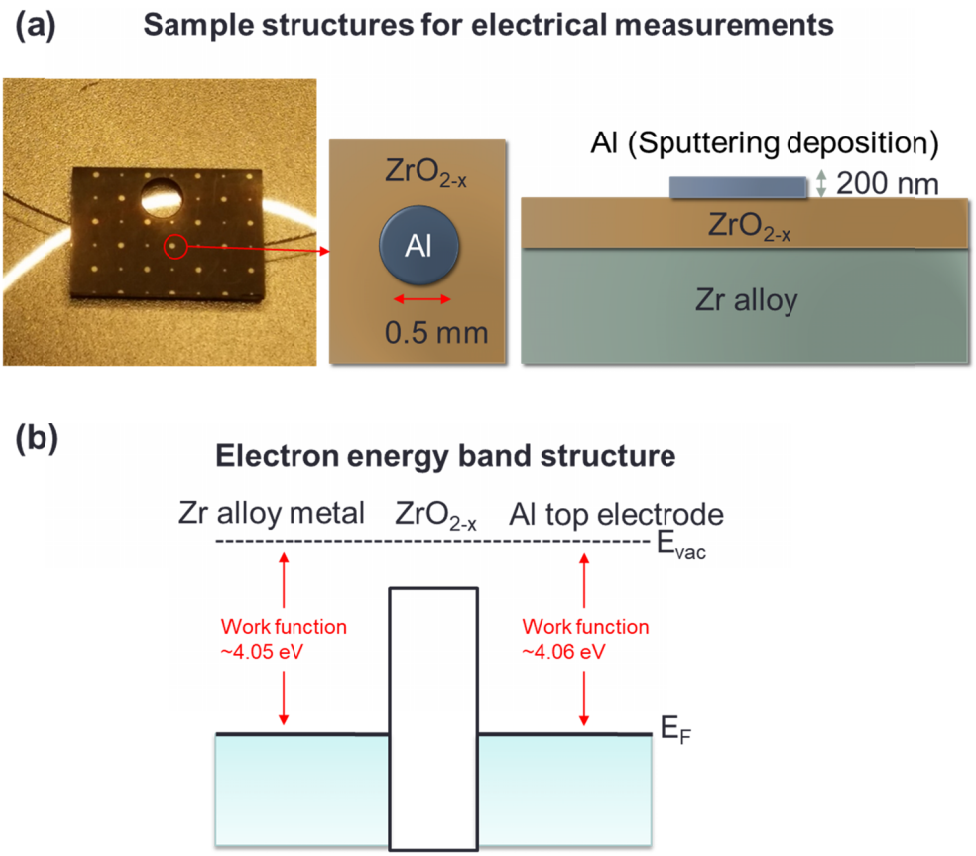

Fig. 1. (a) MIM sample structure for *C-V* and *I-V* measurements. (b) Electron energy band structure of the Zr oxide based MIM capacitor structure used for electrical measurements

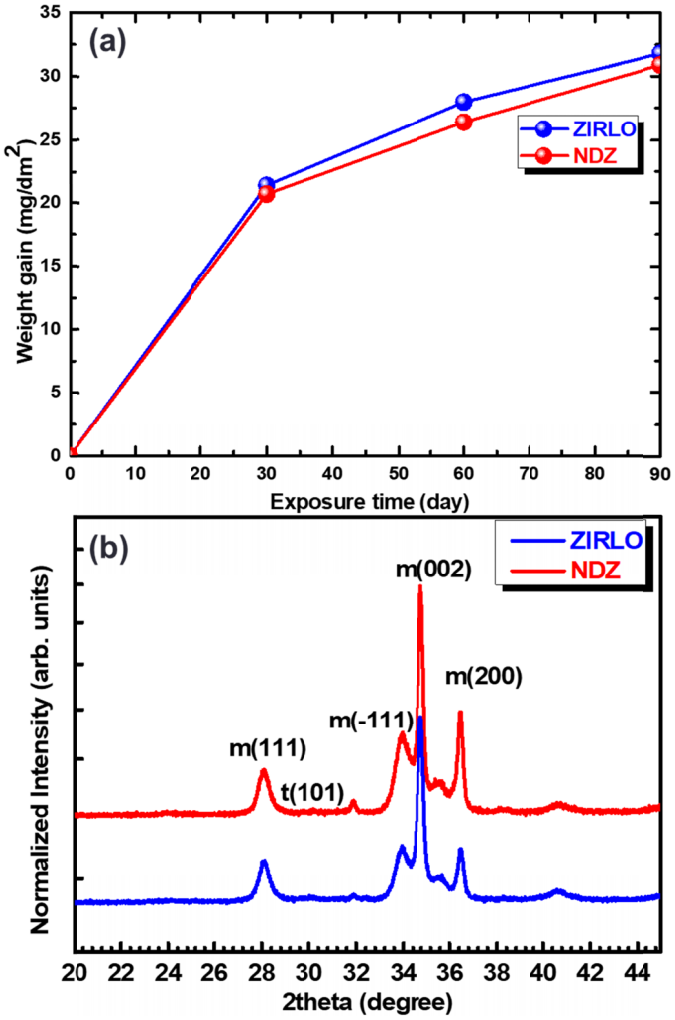

Fig. 2. (a) Weight gain results during corrosion test for the ZIRLO and NDZ. (b) Theta-2 theta XRD results for the Zr oxide layers formed by corrosion

To investigate the electrical properties of the Zr oxides, *C-V* was measured after fabricating top electrode as shown in Fig. 1. The Zr was used as bottom electrode after grinding and polishing the back side to expose the fresh Zr surface. Considering the work function of Zr as 4.05 eV, the aluminum can be an excellent counter electrode to form a symmetric capacitor, because its work function is 4.06 eV. As shown in Fig. 1(b), the device structure can exhibit a MIM capacitor structure due to insulating nature of the Zr oxide layers. Figure 3(a) shows the *C-V* results for the Zr oxides formed on the ZIRLO and NDZ measured at low (10 kHz) and high (1 MHz) frequency between –10 and 10 V. The capacitance value of the Zr oxide showed linear behavior with applied voltage. The dielectric constant of the Zr oxide was estimated from the measured capacitance values based on following equation;

$$C = \varepsilon_r \varepsilon_o \frac{A}{d}$$

where, C is the capacitance, ε_r is relative dielectric constant of the oxide, ε_o is vacuum permittivity of 8.8542×10^{-12} F/m, A is the electrode area, and d is the thickness of the oxide layers.

The estimated dielectric constant values for the Zr oxide on the ZIRLO and NDZ are 11.28 and 11.52, respectively. Even though these values are much lower than 25 which is well-known dielectric constant value of bulk ZrO_2, these are very close to the already reported dielectric constant value 11 for the anodic and thermally formed Zr oxide film [13]. The lower value of dielectric constant for the oxidized Zr than that of bulk or dense ZrO_2 would be due to loss of stoichiometry and defective structures of the oxide layers. Figure 3(b) summarizes the average capacitance values for the samples depending on the frequency. It should be noted that the difference between the capacitances at low and high frequency of the ZIRLO is much larger than that of the NDZ. This would be attributed to the different contribution of the polarization mechanism. There are four basic polarization mechanisms in the materials; electronic, ionic, orientational, and interfacial polarization [14]. Among them, the interfacial polarization contributes to the total polarization only in the low frequency range because the interfacial polarization occurs whenever there is an accumulation of charge at an interface between two materials, in this case, between the metal and oxide layers. The mobile charges can be trapped electrical charge carriers at the defect states or hydrogen ions. The difference between the capacitances at the low and high frequency ranges implies the contribution of the interfacial polarization. the large capacitance

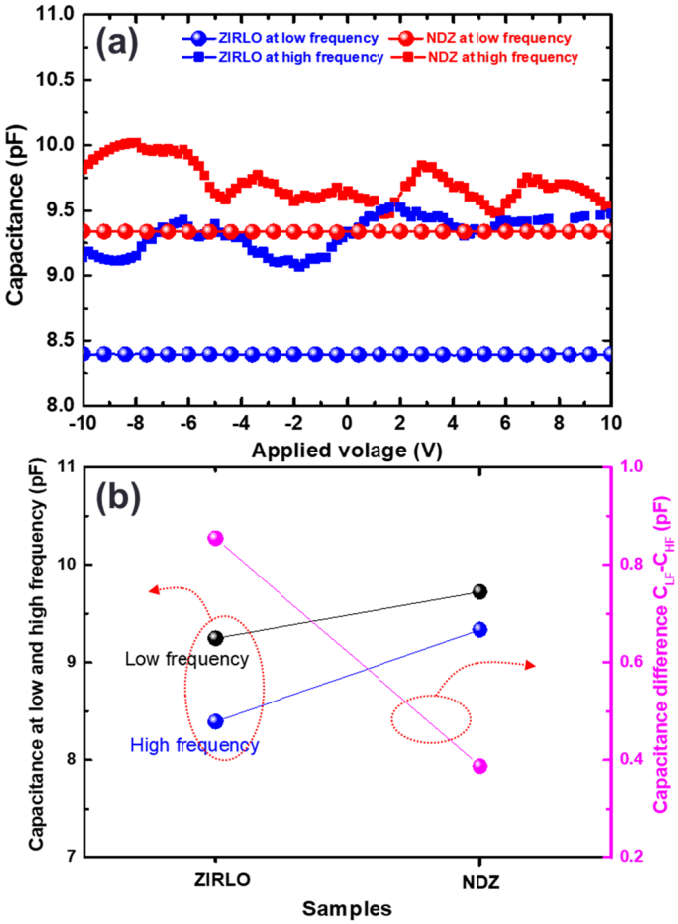

Fig. 3. (a) *C-V* curves for the ZIRLO and NDZ at the low (10 kHz) and high frequency (1 MHz) ranges. (b) Summary of capacitance values at low and high frequency and capacitance difference

difference indicates more contribution of the interfacial polarization due to larger amount of mobile electrical charge carriers. Therefore, this implies that the ZIRLO alloy contains more mobile electrical charge carriers than NDZ, which is coincident with the corrosion results.

To investigate further about the transport behavior of mobile charges in the oxide layer, temperature-dependent *I-V* was measured for the MIM capacitors. As shown in Figs. 4(a) and (b), the ZIRLO and NDZ showed asymmetric *I-V* characteristics, which would be due to non-uniform distribution of defects in the oxide layers. Under the reverse bias condition, more current flows than in forward bias condition. It should be noted that the current increases as temperature increases. In addition, the increment of the current with increasing temperature is larger in the ZIRLO than in the NDZ. This indicates that more charge trap sites exist in the ZIRLO than in NDZ. This coincide with the corrosion test results, which showing better corrosion-resistant property in NDZ than ZIRLO. Therefore, the corrosion behavior could be estimated based on the electrical measurements. To investigate more about the temperature-dependent *I-V* results, *lnJ* vs $1/T$ relation was plotted as shown in Fig. 4(c) and it shows linear relation. This temperature-dependent behavior can be explained as a Poole-Frenkel conduction mechanism, which is one of conduction mechanism through an insulator [13]. As shown in the inset of Fig. 4(c), crystalline defects in Zr oxide forms localized trap energy states within the energy bandgap. The electrons or other electrical charge carriers are generally trapped in these localized state. As temperature increases, random thermal fluctuations can provide enough energy to the electrical charge carriers to escape from its localized state, excited into the conduction band, and finally results in increased current flow. The standard quantitative expression for the Poole-Frenkel effect can be expressed as [15,16];

$$J \propto E \exp\left(\frac{-q(\phi_B - \sqrt{qE/\pi\varepsilon}}{k_B T}\right)$$

where, J is the current density, E is the applied electric field, q is the elementary charge, ϕ_B is the voltage barrier that an electron must cross to move from one atom to another in the crystal, ε is the dynamic permittivity, k_B is Boltzmann's constant, and T is the temperature. This equation implies that the *lnJ* and $1/T$ have linear relation as shown in Fig. 4(c). It should be note that the current increases more drastically in ZIRLO than in NDZ. This indicates that more defective oxide layer was formed within the oxide of the ZIRLO alloy. During corrosion process, transportation of oxygen, hydrogen ions, and electrons between the coolant and Zr alloy cladding layers through the oxide layer determines the corrosion kinetics. Therefore, the capacitive and transportation behavior of electrical charge carriers within the oxide layers can be closely related with the corrosion rate of the Zr alloys. In this way, the corrosion behavior of the Zr alloys can be estimated by only considering the dynamic charge carrier transport behavior at the initial stage.

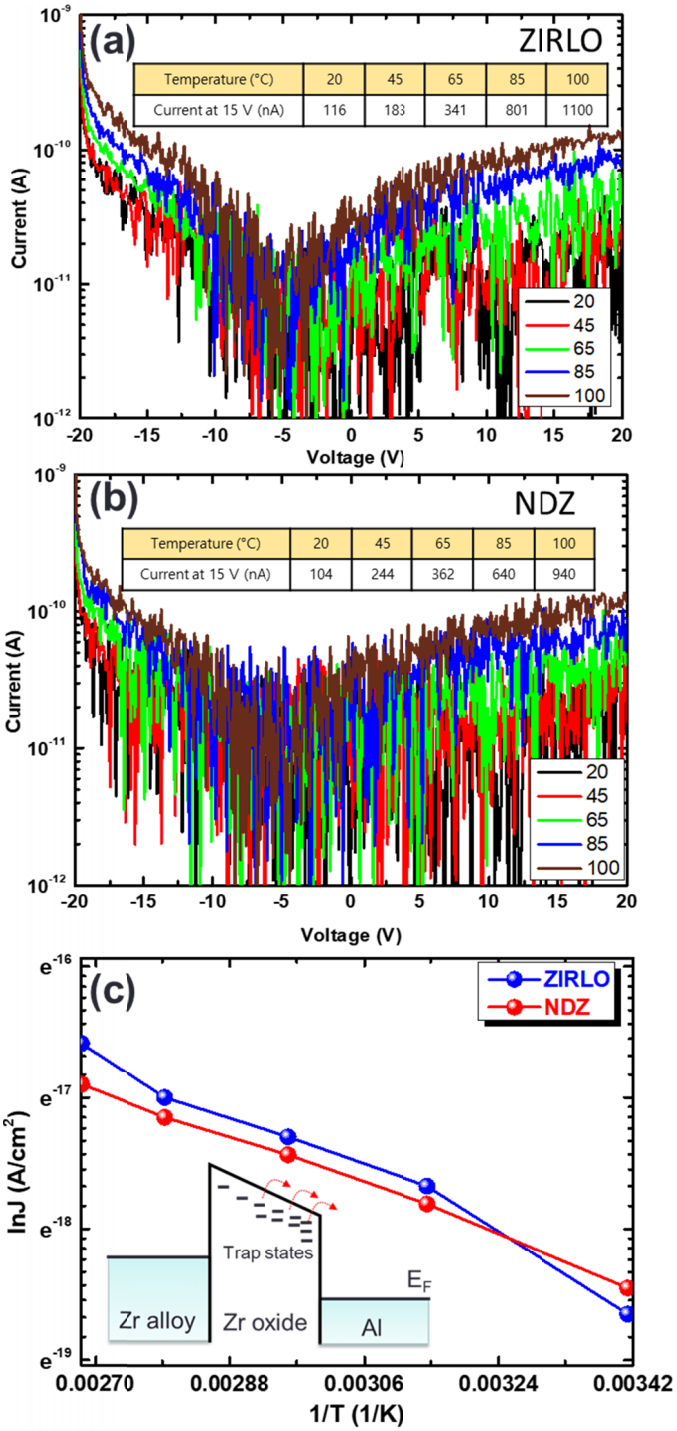

Fig. 4. Temperature-dependent *I-V* curves for the (a) ZIRLO and (b) NDZ. *lnJ* vs $1/T$ relation for the ZIRLO and NDZ. The inset shows electron energy band structure under reverse bias condition which showing a Poole-Frenkel conduction mechanism through Zr oxides

4. Conclusions

In this study, the dynamic charge carrier transport behavior in the Zr oxide based on the frequency-dependent *C-V* and temperature-dependent *I-V* measurements. The Zr oxide was formed on the ZIRLO and newly developed NDZ by corrosion in

the PWR-simulated loop at 360°C. The corrosion test results for 90 days showed that the NDZ exhibits better corrosion resistance than ZIRLO. The estimated dielectric constant values for the Zr oxide on the ZIRLO and NDZ are 11.28 and 11.52, respectively, which are very close to the already reported dielectric constant value 11 for the anodic and thermally formed Zr oxide film. The capacitance difference between low and high frequency was larger in the ZIRLO than in the NDZ, which was attributed to the contribution of the interfacial polarization and implied that the oxide of ZIRLO alloy contained more mobile electrical charge carriers than that of NDZ. In addition, the increment of the current through the oxide layers with increasing temperature is larger in the ZIRLO than in the NDZ, which indicating exist of more charge trap sites in the ZIRLO than in NDZ. These electrical charge carrier transport influenced on the corrosion kinetics. And the capacitive and transportation behavior of electrical charge carriers within the oxide layers can be crucial in estimating the corrosion of Zr alloys at the early stage.

Acknowledgments

This research was supported by Basic Science Research Program through the National Research Foundation of Korea (NRF) funded by the Ministry of Science and ICT of Korean government (No. 2019M2A8A5019865 and 2017M2A8A5015058).

REFERENCES

[1] F. Garzarolli, H. Stehle, E. Steinberg, ASTM STP **1295**, 12 (1996).
[2] A.V. Nikulina, A.M. Vladimir, M.M. Peregud, Y.K. Bibilashvili, V.A. Kotrekhov, A.F. Lositsky, N.V. Kuzmenko, Y.P. Shevnin, V.K. Shamardin, G.P. Kobylyansky, A.E. Novoselov, ASTM STP **1295**, 785 (1996).
[3] J.Y. Park, B.K. Choi, Y.H. Jeong, Y.H. Jung, J. Nucl. Mater. **340**, 237 (2005).
[4] H.G. Kim, J.H. Yang, W.J. Kim, Y.H. Koo, Nucl. Eng. Technol. **48**, 1 (2016).
[5] H.G. Kim, B.K. Choi, Y.H. Jeong, Met. Mater. Int. **15**, 43 (2009).
[6] H. Anada, K. Nomoto, Y. Shida, ASTM STP **1245**, 307 (1994).
[7] G.P. Sabol, ASTM STP **1467**, 3 (2005).
[8] Y.H. Jeong, S.Y. Park, M.H. Lee, B.K. Choi, J.H. Baek, J.Y. Park, J.H. Kim, H.G. Kim, J. Nucl. Sci. Technol. **43**, 977 (2006).
[9] B. Cox, J. Nucl. Mater. **28**, 1 (1968).
[10] B. Cox, J. Nucl. Mater. **29**, 50 (1969).
[11] B. Cox, J.P. Pemsler, J. Nucl. Mater. **28**, 73 (1968).
[12] R.C. Garvie, P.S. Nicholson. J. Am. Ceram. Soc. **55**, 303 (1972).
[13] B. Cox, Third International Congress on Metallic Corrosion, Moscow **4**, 341 (1966).
[14] S.O. Kasap, Principles of Electronic Materials and Devices, New York 2006.
[15] J. Frenkel, Phys. Rev. **54**, 647 (1938).
[16] P. Rottländer, M. Hehn, A. Schuhl, Phys. Rev. B **65**, 054422 (2002).